Acta Crystallographica Section D
Biological Crystallography
ISSN 0907-4449

Combined pseudo-merohedral twinning, non-crystallographic symmetry and pseudo-translation in a monoclinic crystal form of the $\gamma\delta$ T-cell ligand T10

Markus G. Rudolph,[a]*‡ Christer Wingren,[a]§ Michael P. Crowley,[b] Yueh-hsiu Chien[b] and Ian A. Wilson[a]*

[a]Department of Molecular Biology and The Skaggs Institute for Chemical Biology, The Scripps Research Institute, La Jolla, CA 92037, USA, and [b]Program of Immunology and the Department of Microbiology and Immunology, Stanford University, School of Medicine, Stanford, CA 94305, USA

‡ Present address: Department of Molecular Structural Biology, Institute for Microbiology and Genetics, Georg-August University, 37077 Göttingen, Germany.
§ Present addess: Department of Immunotechnology, Lund University, SE-22077 Lund, Sweden.

Correspondence e-mail: markus.rudolph@bio.uni-goettingen.de, wilson@scripps.edu

Received 20 November 2003
Accepted 27 January 2004

PDB Reference: $\gamma\delta$ T-cell ligand T10, 1r3h, r1r3hsf.

T10 is a non-classical class Ib-like major histocompatibility complex (MHC) cell-surface antigen which binds directly to certain $\gamma\delta$ T-cell receptors in the absence of any exogenous and endogenous ligands, such as peculiar lipids or glycolipids. The crystal structure at 2.5 Å resolution of murine T10 was determined by molecular replacement using data from an almost perfectly twinned monoclinic crystal. The space group is $P2_1$, with unit-cell parameters $a = 78.2$, $b = 70.0$, $c = 139.2$ Å, $\beta = 106.8^\circ$. Self-rotation function analysis and various intensity statistics revealed the presence of pseudo-merohedral twinning, but these tests underestimated the true twin fraction of $\alpha \simeq 0.46$. Native Patterson analyses pointed to the presence of pseudo-translation among the four molecules present in the asymmetric unit. Data analysis, structure determination and model refinement are discussed.

1. Introduction

Twinning may be observed in crystalline specimens where two or more crystals of different relative orientations inter-grow to form a larger aggregate (Catti & Ferraris, 1976; Donnay & Donnay, 1974; Friedel, 1926). If the lattices of the individual crystals overlap in three dimensions, the larger aggregate is merohedrally twinned and produces a single diffraction pattern which does not reveal the presence of twinning *per se* (Yeates, 1997; Yeates & Fam, 1999). Hemihedrally twinned crystals are composed of molecules that are organized into two different twin domains (Chandra *et al.*, 1999; Yeates, 1997; Yeates & Fam, 1999) and their diffraction pattern is therefore a superposition of the diffraction pattern of each individual twin domain (Liang *et al.*, 1996; Lietzke *et al.*, 1996). These crystals are described by the symmetry operation necessary to superimpose the twin domains (the twinning operator) and the fractional volume of the less populated twin domain in the crystal, the twin fraction α.

In merohedral twins, the twinning operator introduces additional symmetry that is not part of the true Laue symmetry group of the crystal, but is a symmetry operator of the apparent higher symmetry Laue group of the same crystal system. Thus, merohedral twinning is observed in the tetragonal, trigonal, hexagonal and cubic crystal systems. In pseudo-merohedral twins, the twin operator is not a symmetry operator of a higher symmetry Laue group of the same crystal system, but introduces additional symmetry that suggests a higher Laue symmetry than is possible for the point group of the sample. This rare type of twinning may arise in the monoclinic and orthorhombic crystal systems by equivalence of two unit-cell axes or, in the monoclinic system with b as the unique axis, where the β angle is close to 90°. Finally, it is

possible in $P2$ or $C2$ crystals that an orthorhombic metric is introduced by unit-cell parameters that satisfy the condition $c\cos\beta = -a/2$, *i.e.* the two unit cells of the twin domains share the same a and b axes, but with opposite directions. A twofold rotation about an axis perpendicular to the a and b axes (*i.e.* along c^*) exactly superimposes the two cells. In this case, the axes [1 0 1] and [−1 0 1], *i.e.* the vectors $a + c$ and $-a + c$, have the same length.

Twinned data have been used previously for structure determination of macromolecules by molecular replacement (Breyer *et al.*, 1999; Contreras-Martel *et al.*, 2001; Larsen *et al.*, 2002; Luecke *et al.*, 1998; Rabijns *et al.*, 2001; Redinbo & Yeates, 1993; Taylor *et al.*, 2000; Trame & McKay, 2001), single or multiple isomorphous replacement (Ban *et al.*, 1999; Declercq & Evrard, 2001; Forst *et al.*, 1998; Goldman *et al.*, 1987; Hillig *et al.*, 1999; Mueller, Muller *et al.*, 1999; Mueller, Schubel *et al.*, 1999; Terwisscha van Scheltinga *et al.*, 2001) and also multiple anomalous dispersion (Rudolph *et al.*, 2003; Yang *et al.*, 2000), showing that twinned data complicate structure determination but do not necessarily render it impossible.

Classical MHC class Ia molecules play a key role in immune recognition by presenting peptides on the cell surface to cytotoxic $\alpha\beta$ T-cell receptors (TCRs; Garcia & Teyton, 1998; Mazza *et al.*, 1998; Rudolph & Wilson, 2002). By contrast, many non-classical MHC molecules display specialized antigen-binding properties and have evolved for specific tasks that are distinct from those of classical MHC class Ia (Braud *et al.*, 1999; Shawar *et al.*, 1994; Stroynowski & Lindahl, 1994). The non-classical MHC class Ib molecules T10 and T22 are highly homologous (93% sequence identity) and have been described as specific ligands for $\gamma\delta$ TCRs without the requirement for a bound peptide or other small ligand (Crowley *et al.*, 1997, 2000). In class Ia molecules, the peptide ligand is bound in a deep groove formed between two long α-helices that traverse a β-sheet platform. The crystal structure of T22 has been determined to a resolution of 3.1 Å and revealed a disrupted 'peptide'-binding site with no obvious groove owing primarily to two deletions in the sequence compared with classical peptide-binding MHC molecules (Wingren *et al.*, 2000). The deletions resulted in partial unfolding of one of the α-helices, which instead adopts a loop conformation that appears to be extremely flexible, as judged by its high B values.

Many crystal structures of classical class I and class II MHC molecules were required in order to delineate the general principles for peptide binding and antigen presentation to TCRs. The crystal structure of T10, the second member of this non-classical MHC that binds to $\gamma\delta$ T-cell receptors, was determined to 2.5 Å to improve the resolution over the previously determined T22 and to possibly reveal further insights into the nature and flexibility of the binding groove that differs so significantly from the classical MHC. Unfortunately, the crystals of T10 exhibited a high degree of pseudo-hemihedral twinning, which did not hamper structure determination by molecular replacement but, together with the presence of pseudo-translation, complicated refinement of the model. In this study, we outline the analysis and phasing of the T10 diffraction data from pseudo-merohedrally twinned crystals using molecular replacement.

Table 1
Crystallographic data collection, analysis and structure refinement.

Data collection	
Wavelength (Å)	0.98
Resolution range† (Å)	46.0–2.5 (2.59–2.50)
Unique reflections	46914 (3879)
Completeness (%)	93.5 (78.0)
$R_{\rm sym}$, $P2$‡§ (%)	[6.4] 10.0 (33.2)
$R_{\rm r.i.m.}$, $C222$‡§ (%)	[7.5] 11.0 (24.2)
Average $I/\sigma(I)$†	13.5 (3.7)
Multiplicity of observations†	3.0 (2.3)
Mean $\lvert E^2 - 1\rvert$¶	0.673 (0.736)
$\langle\lvert I\rvert^2\rangle/\langle\lvert I\rvert\rangle^2$††	2.0 (2.0/1.5)
$\langle\lvert F\rvert\rangle^2/\langle\lvert F\rvert^2\rangle$††	0.822 (0.785/0.865)
Refinement	
Resolution range† (Å)	46.0–2.5 (2.61–2.50)
No. reflections/test set†	46904 (3927)/2225 (209)
$R_{\rm cryst}/R_{\rm free}$†‡‡ (%)	23.1 (31.7)/27.2 (38.2)
No. residues/protein atoms	1384/11379
Coordinate error§§ (Å)	0.47
Twin operator/refined twin fraction	$-h, -k, h$ + l/0.46
R.m.s. deviation from ideality	
Bonds (Å)	0.006
Angles (°)	1.3
Dihedrals (°)	28.8
Ramachandran plot¶¶	
Core	71.2
Allowed	25.1
Generous allowed	3.1
Disallowed (%)	0.6
Average B values (Å^2)	25.1 ± 8.4

† Values in parentheses refer to the highest resolution shell. ‡ $R_{\rm sym} = 100\sum_h\sum_i |I_i(h) - \langle I(h)\rangle|/\sum_h\sum_i I_i(h)$, where $I_i(h)$ is the ith measurement of reflection h and $\langle I(h)\rangle$ is the average value of the reflection intensity. $R_{\rm r.i.m.} = 100\sum_h[n/(n-1)]^{1/2}\sum_i |I_i(h) - \langle I(h)\rangle|/\sum_h\sum_i I_i(h)$, where n is the multiplicity of observations. § Values in square brackets refer to the lowest resolution shell: 46.0–5.38 Å for $P2$ and 46.0–6.9 Å for $C222$. The highest resolution shell for $C222$ is 2.55–2.50 Å. ¶ The value in parentheses is the expected value for untwinned data. †† Values in parentheses are the expected values for untwinned/perfectly twinned data. ‡‡ $R_{\rm cryst} = \sum|F_{\rm o}| - |F_{\rm c}|/\sum|F_{\rm o}|$, where $F_{\rm o}$ and $F_{\rm c}$ are the structure-factor amplitudes from the data and the model, respectively. $R_{\rm free}$ is $R_{\rm cryst}$ using a 5% test set of structure factors. §§ Based on a Luzzati plot (Luzzati, 1952). ¶¶ Calculated using *PROCHECK* (Laskowski *et al.*, 1993).

2. Materials and methods

2.1. Protein purification, crystallization and data collection

Murine H-2 T10 was produced, purified from inclusion bodies and refolded as described previously (Crowley *et al.*, 1997). T10 was crystallized from 0.2 M imidazole malate pH 5.2, 11% MPEG 5000, 0.2 M $MgCl_2$. A data set to 2.5 Å resolution (Table 1) was collected from a cryocooled single crystal at 93 K on beamline 9-1 at the Stanford Synchrotron Radiation Laboratory (SSRL). Data reduction was performed using the *HKL* package (Otwinowski & Minor, 1997). Indexing and integration was possible in both primitive monoclinic ($P2$) and C-centred orthorhombic ($C222$) settings, leading to unit-cell parameters a = 78.2, b = 70.0, c = 139.2 Å, β = 106.8° and a = 78.2, b = 266.6, c = 70.0 Å, respectively. The overall and low-resolution scaling statistics for $C222$ were only slightly worse than those for $P2$ (Table 1). The redundancy-

corrected $R_{\rm r.i.m.}$ values (Diederichs & Karplus, 1997) for $C222$ were calculated with *XPREP* (Bruker AXS) from the data reduced in $P2$. This explains the slightly lower value for the high-resolution shell in the $C222$ case compared with $P2$. The presence of a twofold screw axis was established by analysis of the systematically absent reflections from data processed in $P2$, leaving $P2_1$ and $C222_1$ (a minimal non-isomorphic supergroup of $P2_1$) as possible space groups. As discussed below (§3), the true space group is $P2_1$ and the presence of twinning emulates orthorhombic symmetry. The Matthews coefficient (Matthews, 1968) $V_{\rm M} = 2.2$ Å^3 Da^{-1} suggested four molecules in the asymmetric unit with a solvent content of 44%.

2.2. Data analysis

Self-rotation function analysis of the data processed in $P2$ using *POLARRFN* (Collaborative Computational Project, Number 4, 1994) in the resolution range 10–5 Å and with a

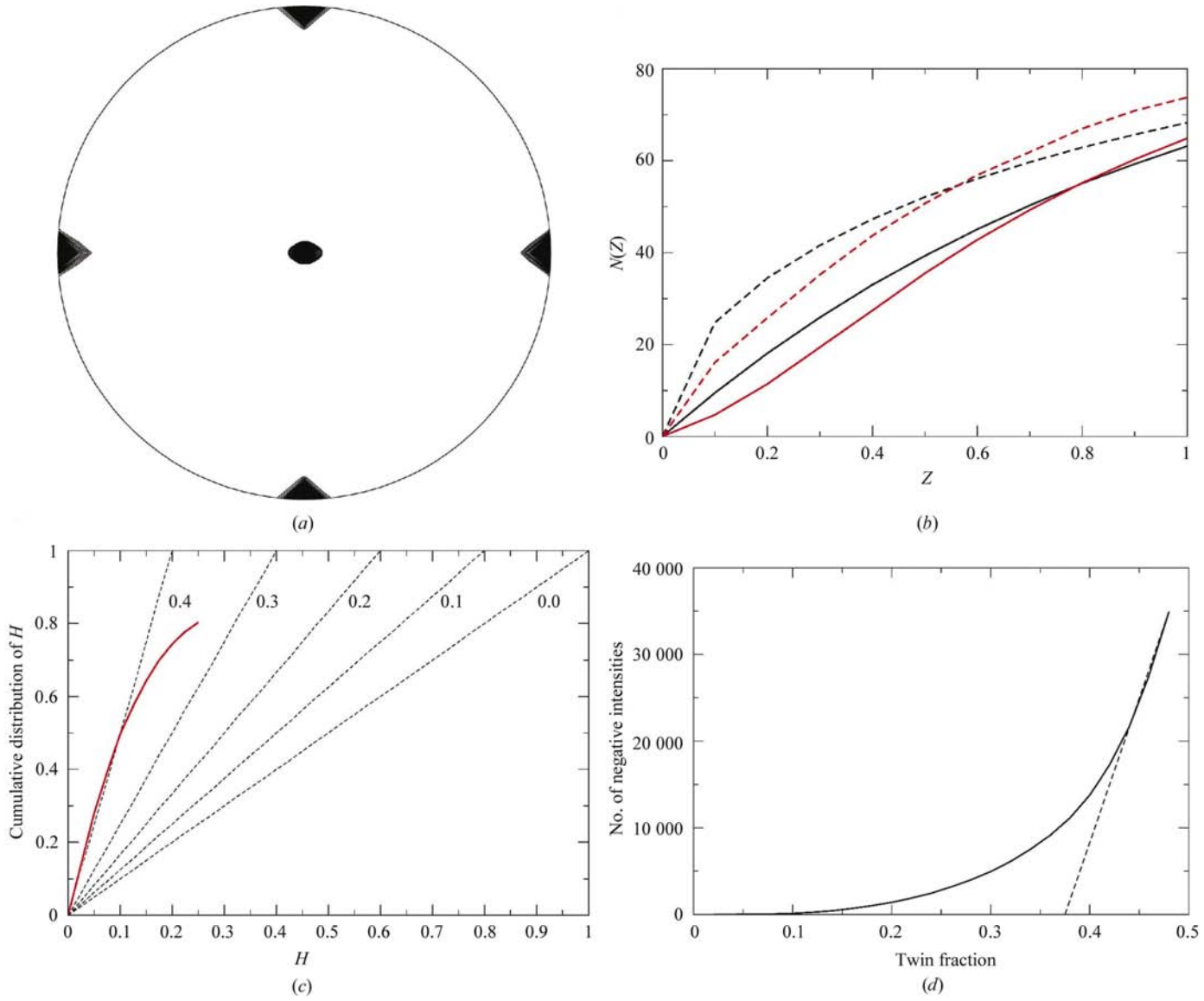

Figure 1
Detection and analysis of twinning. (*a*) Stereographic projection plot of the $\kappa = 180^\circ$ section of the self-rotation function of the native data set. The function was calculated with resolution limits of 15 and 3 Å, a Patterson integration radius of 27 Å and contoured at >40% of the maximum peak height using *POLARRFN* (Collaborative Computational Project, Number 4, 1994). The data were reduced in $P2$, but the plot shows 222 symmetry, with one twofold axis ($\omega = 0$, at the centre) and the other twofold axes ($\omega = 90^\circ$, at the perimeter) having equal heights. Detwinning of the data does not change the plot owing to the presence of a non-crystallographic twofold axis perpendicular to the b axis. (*b*) Cumulative distribution of $Z = I/\langle I\rangle$, where I is the intensity, for the acentric (continuous red line) and centric (dashed red line) T10 data. The theoretical distributions for untwinned data are shown as black lines. The sigmoidal shape of the distribution of the acentric reflections indicates potential twinning. (*c*) Estimation of the twin fraction α by plotting the cumulative fractional intensity difference of acentric twin-related intensities, $H = |I_1 - I_2|/(I_1 + I_2)$, as a function of H (Yeates, 1988). The initial slope of the distribution is a measure of α. The dotted lines represent the expected slopes for the indicated twin fractions. (*d*) Estimation of α by a Britton plot (Britton, 1972; Fisher & Sweet, 1980). The number of negative intensities after detwinning is plotted as a function of the assumed value of α. An overestimation of α will increase the number of negative intensities and the actual value of α is extrapolated from this increase (dotted line). The line is a linear fit of the data with $\alpha \geq 0.44$ and intersects the x axis at $\alpha = 0.37$.

Patterson integration radius of 27 Å showed the presence of a twofold axes perpendicular to the crystallographic *b* axis, indicating possible higher (orthorhombic) space-group symmetry or the presence of a non-crystallographic (NCS) axis perpendicular to, but not necessarily intersecting, the unique *b* axis. The cumulative intensity distributions calculated with *TRUNCATE* (Collaborative Computational Project, Number 4, 1994) and reduced $|E^2 - 1|$ values from *XPREP* indicated hemihedral twinning in space group $P2_1$ (Fig. 1, Table 1), which is not normally possible in the monoclinic system. The twin law $-h, -k, h+1$ describes a real-space rotation about an axis perpendicular to the crystallographic twofold. The twin fraction was estimated to be about 0.4 by the cumulative distribution of *H* (Yeates, 1988) and around 0.37 by the Britton plot (Fisher & Sweet, 1980). Further analysis of the native Patterson maps in *P*2 showed the presence of two peaks of 27σ and 23σ height centred at fractional coordinates 0.0, 0.07, 0.5 and 0.5, 0.07, 0.5, respectively, which suggested pseudo-translational symmetry (Fig. 3).

2.3. Structure determination and refinement

For structure determination using molecular replacement, the untreated twinned data were used. As the space group was not assigned at this point, systematic molecular-replacement approaches which varied the resolution ranges for rotation and translation and the Patterson integration radius using *AMoRe* (Collaborative Computational Project, Number 4, 1994) and *COMO* (Jogl *et al.*, 2001) were carried out in space groups $P2_1$ and $C222_1$ (four and two molecules per asymmetric unit, respectively) using the structure of the highly homologous T22 molecule as a search model (Wingren *et al.*, 2000). Only in space group $P2_1$ were rotation and translation solutions found that showed reasonable crystal packing and which were consistent with the observed non-crystallographic symmetry. The initial model for refinement was derived using *COMO* with a resolution range of 10–3.5 Å for rotation and translation searches and rigid-body refinement and a Patterson integration radius of 35 Å. Two strong rotation-function peaks of 12.1σ and 11.7σ were related by a 180° rotation, with the next (false) rotation solution being 6.4σ. The translation search resulted in two pairs of NCS-related molecules separated by a pure translation according to one of the two largest peaks in the native Patterson map. This model displayed a correlation coefficient of 0.39 and an *R* value of 51.1% after rigid-body refinement.

Further rigid-body refinement to 3.5 Å resolution, which modelled three domains per MHC molecule, followed by separate positional, simulated-annealing and temperature-factor refinement to 2.5 Å resolution, was performed in *CNS* (Brünger *et al.*, 1998) against intensities using protocols for twinned data. The twin fraction was fixed at a cautiously low value (slightly lower than that estimated from the Britton plot) of $\alpha = 0.35$. Except for rigid-body refinement, all refinement procedures included separate NCS restraints for the main-chain and side-chain atoms of each of the three domains in an MHC molecule. The test set was chosen so as to avoid twin-related reflections being present in both the test set and working set, which would invalidate $R_{\rm free}$ as an independent monitor of the refinement progress. The model was rebuilt into σ_A-weighted $3F_{\rm o} - 2F_{\rm c}$ electron-density maps using *O* (Jones *et al.*, 1991). After convergence in *CNS* ($R_{\rm cryst} = 30\%$, $R_{\rm free} = 32\%$), refinement of the twin fraction was performed with *SHELXL* (Sheldrick & Schneider, 1997). The test set was kept intact during all refinement steps in all programs. Using the refined twin fraction of 0.46 in *CNS*, the final model produced an $R_{\rm cryst}$ of 23.1% and an $R_{\rm free}$ of 27.2% (Table 1). The model includes all residues except residues 148–157 in molecules 1–4 and residues 127–129 in molecule 4, which showed no interpretable electron density. Two additional C-terminal residues (274–275) were visible in molecules 1 and 3, but not in molecules 2 and 4. Only 71.2% of all residues are in the most favourable regions of the Ramachandran plot (Table 1); however, this is still within the confidence interval given in *PROCHECK* (Laskowski *et al.*, 1993). As near-perfect twinning effectively halves the number of observed reflection intensities at any given resolution, the 2.5 Å resolution T10 data essentially has the same information content as untwinned data at 3.1 Å resolution. Despite strong NCS restraints, this diminished observable-to-parameter ratio explains the rather unstable refinement that led to the suboptimal geometry of the T10 model. Similar results have been obtained for the twinned structures in PDB entries 1irm (2.55 Å resolution; $R_{\rm free} = 30.7\%$; 69.9% of all residues in the most favourable regions of the Ramachandran plot) and 1k4s (3.2 Å resolution; $R_{\rm free} = 22.2\%$; 78.1% of all residues in the most favourable regions of the Ramachandran plot).

3. Results and discussion

3.1. Detection of twinning in crystals of T10

A number of warning signs for twinning have been compiled (Herbst-Irmer & Sheldrick, 1998) and include apparent higher symmetry owing to the twin operator, which introduces additional symmetry that is not part of the Laue symmetry of the space group. The first indication of possible hemihedral twinning in T10 crystals was the observation that the data could be indexed, processed and scaled with comparable overall $R_{\rm sym}$ values in $P2_1$ and $C222_1$. In addition, resolution-dependent inspection of $R_{\rm sym}$ revealed no gross differences in data reduction between the two space groups, as found in a case for the tetragonal crystal system (Rudolph *et al.*, 2003). Calculation of the packing density assuming four molecules in the asymmetric unit yielded a Matthews coefficient (Matthews, 1968) of $V_{\rm M} = 2.2\ \text{Å}^3\ \text{Da}^{-1}$ (44% solvent content) for the $P2_1$ case. This even number of molecules seems reasonable because in the $C222_1$ setting the volume of the asymmetric unit is only half that of the $P2_1$ unit cell, leaving the packing density unchanged if two molecules per $C222_1$ asymmetric unit are assumed. Thus, packing-density considerations did not provide obvious indications of twinning and the space-group ambiguity had to be resolved during structure determination.

Further analysis of the diffraction data using *XPREP* (Bruker AXS) revealed a lower mean $|E^2 - 1|$ value of 0.673 for the T10 data set than expected for non-centrosymmetric space groups (0.736; Table 1), which represents another hallmark of twinning (Herbst-Irmer & Sheldrick, 1998). The presence of pseudo-222 symmetry is apparent from a self-rotation function analysis of the data that were reduced in *P*2 (Fig. 1*a*). The $\kappa = 180^\circ$ section shows twofold axes perpendicular to the crystallographic twofold axis. A further indication for the presence of hemihedral twinning is an abnormal distribution of $Z = I/\langle I\rangle$. The cumulative intensity distribution of the T10 data, as calculated by *TRUNCATE* (Collaborative Computational Project, Number 4, 1994), is sigmoidal in shape compared with the expected distribution of untwinned data (Fig. 1*b*), further pointing to twinned crystals. Only few possibilities exist for a monoclinic system to become twinned and thus to emulate an orthorhombic metric. A relatively common situation seems to be a monoclinic cell with $a \simeq c$ (Yang *et al.*, 2000) or any monoclinic cell with a β angle close to 90° (Larsen *et al.*, 2002). A further possibility arises where two monoclinic cells have coincident *a* and *b* axes with opposite directions that can be superimposed by a twofold rotation about an axis perpendicular to *a* and *b*. Such a case was recently reported (Declercq & Evrard, 2001) and applies to the T10 case presented here (Fig. 2*a*). This twofold axis runs parallel to the *b* axis of the emulated orthorhombic unit cell (dashed line in Fig. 2*a*), which is the *c** direction of the monoclinic cell, leading to the twin law $-h, -k, h + l$. The NCS axes in the asymmetric unit of T10 are parallel to this twin operation, indicating that the NCS rotation apparently promotes the twinning rotation.

To assess the twin fraction of the T10 data, different twinning tests were employed (Kahlenberg, 1999) using the programs *CNS* (Brünger *et al.*, 1998) and *DETWIN* (Collaborative Computational Project, Number 4, 1994). For acentric untwinned data, the second moment, *i.e.* the expected ratio of the average-squared intensity to the square of the average intensities ($\langle I^2\rangle/\langle|I|\rangle^2$) is 2; for perfectly twinned data, it is 1.5. The T10 data set value was 2.0, suggesting no twinning at all. However, a related value, $\langle|F|\rangle^2/\langle F^2\rangle$, should be 0.785 for untwinned and 0.865 for perfectly twinned data. For T10 it is 0.822, pointing to the presence of partial twinning with a high twin fraction. A possible explanation for this discrepancy in the twinning tests is the presence of pseudo-translation (see below) in the T10 crystals, which results in ∼5.5% of the reflections being very weak, while the same percentage is stronger than expected (see below). These systematic changes in the intensity statistics may skew the results of intensity-based twinning tests. Partial twinning tests in point group 2 with the presence of pseudo-merohedral twinning are not supported by *CNS*, *XPREP* or the twinning server (Yeates, 1997). To assess the twin fraction, a test for partial twinning using the cumulative distribution of *H* (Yeates, 1988), where $H = |I_{obs1} - I_{obs2}|/(I_{obs1} + I_{obs2})$, was performed with *DETWIN* (Collaborative Computational Project, Number 4, 1994), yielding a twin fraction estimate of 0.40 (Fig. 1*c*). This value is slightly larger than the twin fraction of 0.37 estimated from the Britton plot (Fisher & Sweet, 1980) (Fig. 1*d*). However, both tests underestimated the true twin fraction (0.46) considerably, as inferred by atomic refinement.

3.2. Structure determination using twinned data

The $\kappa = 180^\circ$ section of the self-rotation function in *P*2 showed strong twofold-symmetry elements perpendicular to the crystallographic twofold. As no translational information is present in a self-rotation function, the additional twofolds may or may not intersect with each other. In the first case, this

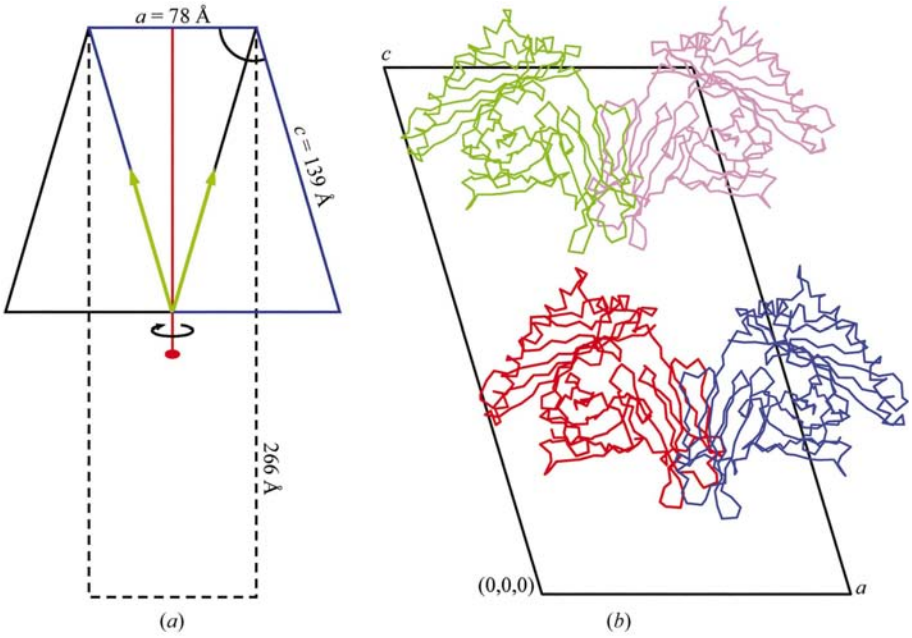

Figure 2
Characteristics of the monoclinic T10 crystal. (*a*) Arrangement of the $P2_1$ cell to allow twinning and emulation of the $C222_1$ cell. The unit cell (blue) is projected along the *b* axis. A 180° rotation of the monoclinic cell about an axis perpendicular to the *a* and *b* axes (red) leads to complete superposition of the two primitive lattices according to the relation $c\cos\beta = -a/2$. The cell in the other twin domain is drawn in black. The effect of the twin operator is to emulate pseudo-centring and the resulting $C222_1$ cell (a = 78, b = 266 Å) is indicated as a dashed line. A pseudo-translation vector, whose projection lies on the *c* axis of the unit cell shown in blue, is duplicated owing to the twin operator (Fig. 3), but otherwise pseudo-translation and twinning are independent of each other. Both vectors are indicated as green arrows. (*b*) The four molecules in the asymmetric unit are shown as C^α traces with the unit cell projected along the *b* axis. Each T10 heterodimer is coloured individually. The molecules in blue and red and the molecules in red and green are related by a pseudo-translation vector of fractional coordinates 0.0, 0.07, 0.5. Note that the second pseudo-translation vector (0.5, 0.07, 0.5) in the native Patterson map (Fig. 3) cannot be reproduced by the model, as it only represents the solution for one twin domain.

could lead to true crystallographic symmetry in an orthorhombic setting, while in the second case the additional symmetry would be local. Molecular replacement in space group $P2_1$ with T22 as the search model using *AMoRe* (Collaborative Computational Project, Number 4, 1994) or *COMO* (Jogl *et al.*, 2001) yielded two clear rotation solutions which were related by a 180° rotation in accord with the presence of twofold NCS as apparent from the self-rotation function. However, although two strong translation-function solutions were found by *AMoRe*, no reasonable crystal packing could be obtained from most of the solutions. The program *COMO*, which contains a built-in packing-evaluation function, found a consistent set of four molecules with only a single translation-function solution (Fig. 2*b*). Despite the very similar scaling statistics of the data in space groups $P2_1$ and $C222_1$ (Table 1), no physically plausible solutions for two molecules in the asymmetric unit were found by any program in space group $C222_1$, confirming $P2_1$ as the correct space group with a high degree of twinning that leads to pseudo-orthorhombic symmetry.

A further test for $C222_1$ being the incorrect space group is whether the molecular-replacement solution in $P2_1$ does or does not fulfil orthorhombic symmetry. *XPREP* was used to calculate structure factors from an initial round of *SHELXL* refinement in $P2_1$, which did not include twin refinement. Merging these calculated data in space group $C222_1$ resulted in a very high $R_{\rm r.i.m.}$ value of 42% that would exclude orthorhombic symmetry and again confirmed monoclinic $P2_1$ as the correct space group. The correct solution then arises from four molecules arranged in two pairs with twofold symmetry. The pairs are related to each other by a pseudo-translation vector of fractional coordinates 0, 0.07, 0.5 (Fig. 2*b*).

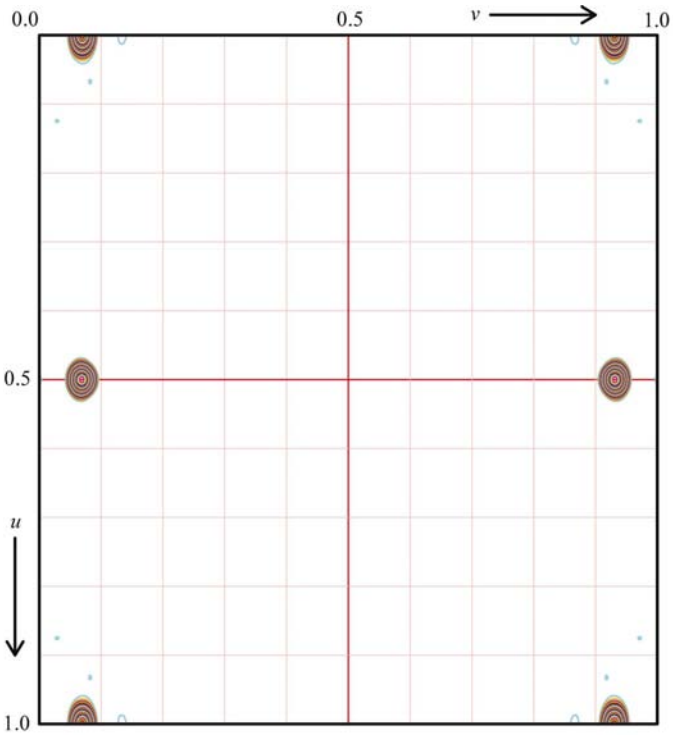

Figure 3
Detection of pseudo-translation in T10 crystals. The plot shows the native Patterson calculated at 2.5 Å resolution at section $w = 0.5$ with a contour level of 2σ. The two pseudo-translation vectors at fractional coordinates 0.0, 0.07, 0.5 and 0.5, 0.07, 0.5 and symmetry-related peaks are visible.

Analysis of the native Patterson map calculated in $P2_1$ to a resolution of 2.5 Å revealed two crystallographically independent peaks at fractional coordinates 0, 0.07, 0.5 and 0.5, 0.07, 0.5 of 27σ and 23σ, respectively. While the first peak is reproduced by the molecular-replacement solution, the second peak is a result of the twinning (see below). This pseudo-translation is also confirmed by calculation of the effect of the pseudo-translation on the intensity distribution of the data (Chook *et al.*, 1998). Calculation of the change of structure factors arising from a translation of 0, 0.07, 0.5 (*i.e.* without taking twinning into account) reveals that reflections h, $k = 14n$, $l = 2n + 1$ and h, $k = 7(2n + 1)$, $l = 2n$ should be systematically weak, while reflections with h, $k = 14n$, $l = 2n$ and h, $k = 7(2n + 1)$, $l = 2n + 1$ should be systematically strong. The reflections are weak and not absent because 0.07 is only approximately 1/14, so that the structure factor for a reflection with k being a multiple of 14 will not be exactly zero. This is indeed the case, as the mean intensities are 2695 (for 914 reflections) and 2194 (for 1679 reflections) for the weak reflections, and 3703 (for 1689 reflections) and 4950 (for 920 reflections) for the strong reflections, with the mean intensity of the data being 3200 (for 46 904 reflections). However, twinning will also affect the reflection intensities, which can be predicted by a similar treatment with the second pseudo-translation. This calculation predicts that some of the systematically stronger reflections arising from the first translation should again become weaker owing to twinning. This change in reflection intensities towards 'normal' values is a result of the weighted averaging of reflection intensities by twinning (see below), but in the T10 case it does not mask the presence of pseudo-translation (Fig. 3).

As expected, the pseudo-translation peaks were also the strongest solutions for the molecular-replacement translation function, but only the first slightly stronger translation led to successful structure determination and refinement. The fractional ratio of the signal heights of the pseudo-translation peaks in the Patterson map [(23/(27 + 23) = 0.46] does not change over the resolution range 46.0–4.0 to 46.0–2.5 Å and is remarkably close to the final refined twin fraction (Table 1). Indeed, the twin operator which relates the two twin domains by a rotation about an axis perpendicular to the crystallographic $P2_1$ b axis (Fig. 2*a*) copies the pseudo-translation of fractional coordinates 0, 0.07, 0.5 to 0.5, −0.07, 0.5, which is symmetry-related to the translation 0.5, 0.07, 0.5 seen in the Patterson map (Fig. 3). In general, a Patterson map of a twinned crystal contains information for both twin domains. If pseudo-translation is present in an untwinned crystal, the corresponding vector will appear twice in the native Patterson map of a twinned crystal (Fig. 2*a*), provided that the pseudo-translational vector and the vector defined by the twin operator are not collinear. Thus, the strongest translation-function solutions in a molecular-replacement procedure will also be duplicated and molecules will be fit in each of the two

twin domains, resulting in many solutions with physically impossible packing.

The independence of the Patterson maps of the individual twin domains, *i.e.* the absence of cross-peaks between them, raises the possibility of another twinning test. If the Patterson were from an untwinned specimen, a strong third peak (>23σ) at a position corresponding to the vector difference between the two observed peaks (0, 0.07, 0.5 and 0.5, 0.07, 0.5) would be expected at 0.5, 0, 0. This peak is present at only 4σ in the Patterson map of the T10 crystal, further confirming the presence of twinning.

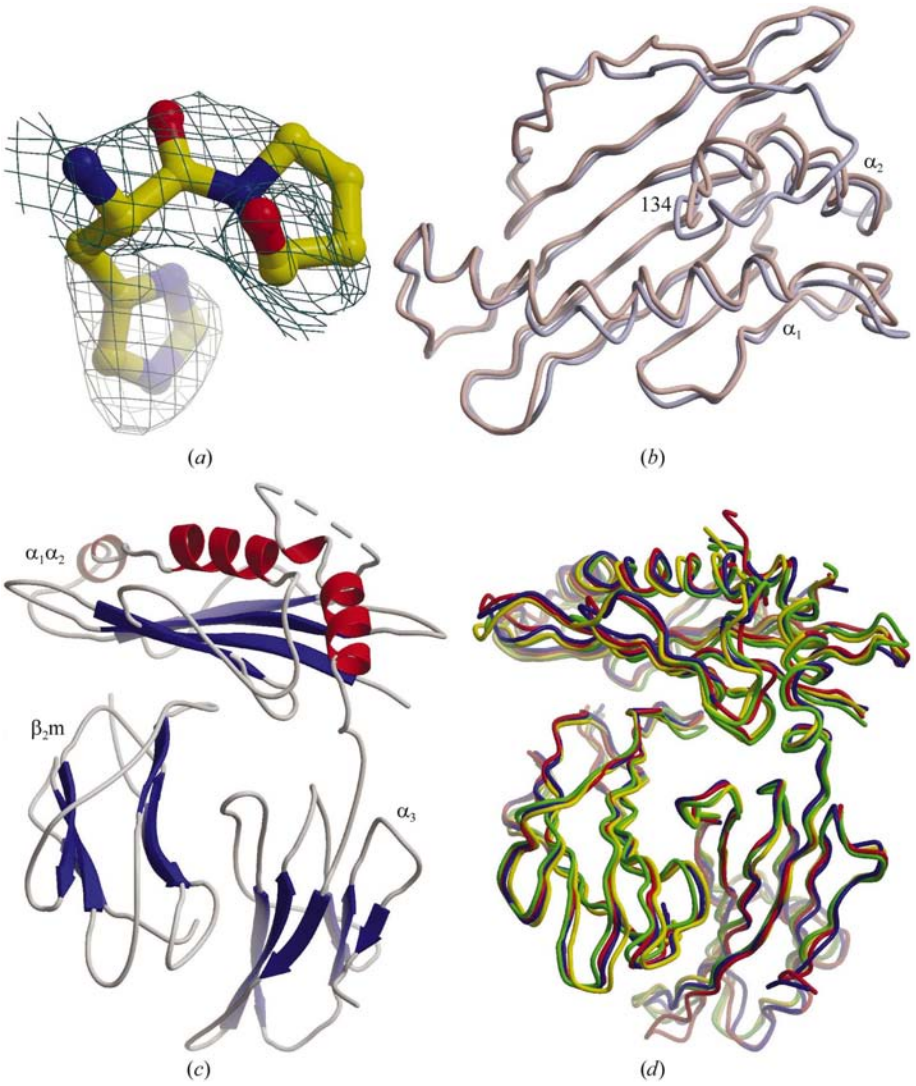

Figure 4
T10 structure and electron density. (*a*) The σ_A-weighted $3F_o - 2F_c$ electron-density map contoured at 1.5σ of the His31–Pro32 region in the β_2m molecule of T10 shows the presence of a *cis*-peptide bond which was not modelled in the lower resolution T22 structure. (*b*) Superposition of the ligand-binding site of T10 (flesh coloured) and T22 (pale blue) shows that both MHC-like molecules are very similar. (*c*) Ribbon representation of the T10 model. The β-strands in the left panel are coloured blue, α-helices red and loop regions grey. The MHC-like domains are labelled. The loop region in T10, which replaces the first half of the α_2-helical segments, was not visible in the electron-density maps and is drawn as a dashed line. The right panel shows an overlay of the four molecules in the asymmetric unit. Each heterodimer is individually coloured.

3.3. Refinement against twinned data and model analysis

While detwinning of intensities is common practice for structure-determination purposes, refinement against detwinned data is not recommended owing to the systematic increase in the associated intensity errors (Rudolph *et al.*, 2003). With a twin fraction of 0.46 and assuming that the mean intensity errors of the twin-related reflections are of the same order, the error increase owing to detwinning is $1/(1 - 2\alpha)$ = 12.5-fold. Consequently, the electron-density maps calculated with detwinned structure-factor amplitudes and model phases were of lower quality than with twinned data (not shown). Thus, *CNS* and *SHELXL*97, which can directly refine against twinned data, were considered for refinement of the T10 model. The first refinement cycles were performed in *CNS* using a fixed twin fraction of α = 0.35 (slightly lower than estimated from the Britton plot) and the protocols for hemihedrally twinned data. However, the R_{free} value stalled at unacceptably high values (R_{free} = 32%) for this resolution (2.5 Å). Therefore, refinement was continued using *SHELXL*97 (Sheldrick & Schneider, 1997), which simultaneously refines the coordinates, the B values and the twin fraction. As 2.5 Å is at the lower resolution limit for this program, only rigid-body refinement using AFIX keywords was performed. The twin fraction, which was fixed in *CNS* at α = 0.35, refined to a value of 0.46, which was then used in further rounds of refinement in *CNS*. This refinement strategy converged to an R_{free} of 27.2% and produced a model (Fig. 4) with reasonable stereochemical properties (Table 1). Although the test set of reflections for cross-validation was selected to avoid the presence of twin-related reflections in both the test and working set, it is likely that the final R_{free} value is an underestimate, as the test set is not entirely independent of the working set owing to the presence of NCS and pseudo-translation (Tickle *et al.*, 1998). The final refined twin fraction of 0.46, which is close to perfect twinning, was expected from the highly similar R_{sym} values of data scaled in $P2_1$ and in $C222_1$. It also appears that in the combined presence of pseudo-merohedral twinning and pseudo-translation, the twin fraction estimates from the Britton plot (0.37) and the cumulative distribution of H (0.40) are out by up to 13–20%. Whether this observation is of more general validity remains to be determined.

Analysis of the T10 electron-density maps revealed features that were not resolved in the 3.1 Å resolution T22 maps. New findings include the identification of two prolyl *cis*-peptide bonds, one in the T10 heavy chain and one in β_2m (Fig. 4*a*). These particular *cis*-peptide bonds are typically found in class I MHC molecules (Madden, 1995). As the β_2m in T10 is the same as in other class I MHC molecules, a His31–Pro32 *cis*-peptide bond was expected. The presence of the heavy-chain Phe209–Pro210 *cis*-peptide bond in the α_3 domain confirms that in T10, as in T22, the MHC-like structure is generally retained, while variations in the binding groove alter its ligand-binding capabilities.

The C^{α} atoms of the four molecules in the T10 asymmetric unit overlay with r.m.s.d. (root-mean-square deviation) values of $\leq$1.4 Å, with the main differences in solvent-exposed loop regions (Fig. 4*b*). As there are significant variations in orientation of the $\alpha_1\alpha_2$, α_3 and β_2m domains, this r.m.s.d. value is an upper limit. Overlay of the individual domains resulted in r.m.s.d. values of 1.04 Å for the $\alpha_1\alpha_2$ domains, 0.86 Å for the α_3 domains and 0.54 Å for the β_2m domains. No density was visible for the region 148–157 in any molecule of the asymmetric unit. These loop regions also showed high *B* values in the T22 structure, indicating conformational flexibility in these $\gamma\delta$ T-cell class Ib ligands. Whether these loop regions adopt a defined structure upon TCR engagement will require crystal structure determination of a complex with their respective TCRs.

4. Conclusions

Recently, Declercq and Evrard described a twinned monoclinic crystal form of human peroxiredoxin 5 (Declercq & Evrard, 2001). Similar to the T10 case, the peroxiredoxin 5 crystal belonged to space group $P2_1$ and pseudo-merohedral twinning was possible owing to the peculiar unit-cell parameters, which exhibited pseudo-orthorhombic symmetry owing to exact overlap of the cell after a twofold rotation about an axis perpendicular to the *a* and *b* axes. In contrast to T10, the second moments of both intensity and structure-factor amplitude clearly showed the presence of twinning in the peroxiredoxin 5 data. Detwinning also shifted the second moment to the expected value (Declercq & Evrard, 2001) despite the presence of pseudo-translation, which rules out the possibility that pseudo-translation skews the second moment to values that generally mask the presence of twinning. Also in contrast to T10, reduction of the native peroxiredoxin 5 data in the higher symmetry space group $C222_1$ resulted in unacceptably high $R_{\rm sym}$ values because of the low twin fraction (0.24). The twin fraction of 0.46 of the T10 data is close to perfect twinning, explaining the low overall $R_{\rm sym}$ for data reduction in both $P2_1$ and $C222_1$ space groups. As in the classic merohedral twinning case, a high twin fraction can mask twinning and may lead to a wrong space-group choice more readily than with crystals that are only slightly twinned.

A search of the PDB for possible monoclinic twins similar to T10 revealed two additional cases where twinning may be present in the data but might have been overlooked during structure determination. The unit-cell parameters of 2352 entries with space group $P2_1$ were tested as to whether they fulfilled the relation $(2c\cos\beta)/a = -1$. Structures whose unit-cell parameters fulfilled this condition but which had a β-angle near 120° or had two equal cell edges were disregarded as they emulate hexagonal or tetragonal metrics, respectively. 77 structures remained with unit-cell parameters that could allow twinning, judged by their values of $(2c\cos\beta)/a$ being within the interval [−1.04 to −0.97]. From the 31 data sets that were available for analysis, three (PDB codes 1igj, 1jch and 1yfo) tested positive for the presence of orthorhombic symmetry as judged by self-rotation functions. Further tests for twinning using cumulative intensity distributions calculated by *TRUNCATE* (which also tests unit-cell parameters for the above relation) and comparison of potentially twin-related reflections using *DETWIN* (Collaborative Computational Project, Number 4, 1994) strongly suggested the presence of such twinning. In the case of 1igj, twinning was considered during refinement and the twin fraction was estimated to be 0.43 (Jeffrey *et al.*, 1993), while in the other two cases twinning may have gone unnoticed. Although NCS is present in the asymmetric unit of 1yfo and the similarity between potentially twin-related reflections weakens somewhat when higher resolution reflections are compared ($\alpha = 0.25$ at 4 Å resolution compared with $\alpha = 0.15$ at the high-resolution limit of 2.25 Å), the cumulative fractional intensity differences *H* indicate an overall twin fraction of ∼0.3. Thus, although pseudo-merohedral twinning seems to be relatively rare in crystals of macromolecules, it should be standard practice to test for the presence of twinning in data sets where initial space-group assignment would not normally indicate twinning as a possible option.

We thank the staff at SSRL beamline 9-1 for support during synchrotron data collection, and Regine Herbst-Irmer, Xiaoping Dai, Jean-Paul Declercq and Robyn Stanfield for helpful discussions. This study was supported by NIH grant CA58896 (IAW) and postdoctoral fellowships from the German Academic Exchange Service and the Skaggs Institute (MGR). This is publication 16159-MB from the Scripps Research Institute.

References

Ban, N., Nissen, P., Hansen, J., Capel, M., Moore, P. B. & Steitz, T. A. (1999). *Nature (London)*, **400**, 841–847.
Braud, V. M., Allan, D. S. & McMichael, A. J. (1999). *Curr. Opin. Immunol.* **11**, 100–108.
Breyer, W. A., Kingston, R. L., Anderson, B. F. & Baker, E. N. (1999). *Acta Cryst.* D**55**, 129–138.
Britton, D. (1972). *Acta Cryst.* A**28**, 296–297.
Brünger, A. T., Adams, P. D., Clore, G. M., DeLano, W. L., Gros, P., Grosse-Kunstleve, R. W., Jiang, J.-S., Kuszewski, J., Nilges, M., Pannu, N. S., Read, R. J., Rice, L. M., Simonson, T. & Warren, G. L. (1998). *Acta Cryst.* D**54**, 905–921.
Catti, M. & Ferraris, G. (1976). *Acta Cryst.* A**32**, 163–165.
Chandra, N., Acharya, K. R. & Moody, P. C. (1999). *Acta Cryst.* D**55**, 1750–1758.

Chook, Y. M., Lipscomb, W. N. & Ke, H. (1998). *Acta Cryst.* D**54**, 822–827.
Collaborative Computational Project, Number 4 (1994). *Acta Cryst.* D**50**, 760–763.
Contreras-Martel, C., Martinez-Oyanedel, J., Bunster, M., Legrand, P., Piras, C., Vernede, X. & Fontecilla-Camps, J. C. (2001). *Acta Cryst.* D**57**, 52–60.
Crowley, M. P., Fahrer, A. M., Baumgarth, N., Hampl, J., Gutgemann, I., Teyton, L. & Chien, Y. (2000). *Science*, **287**, 314–316.
Crowley, M. P., Reich, Z., Mavaddat, N., Altman, J. D. & Chien, Y. (1997). *J. Exp. Med.* **185**, 1223–1230.
Declercq, J. P. & Evrard, C. (2001). *Acta Cryst.* D**57**, 1829–1835.
Diederichs, K. & Karplus, P. A. (1997). *Nature Struct. Biol.* **4**, 269–275.
Donnay, G. & Donnay, J. D. H. (1974). *Can. Mineral.* **12**, 422–425.
Fisher, R. G. & Sweet, R. M. (1980). *Acta Cryst.* A**36**, 755–760.
Forst, D., Welte, W., Wacker, T. & Diederichs, K. (1998). *Nature Struct. Biol.* **5**, 37–46.
Friedel, G. (1926). *Leçons de Cristallographie.* Nancy/Paris/Strasbourg: Berger-Leurault.
Garcia, K. C. & Teyton, L. (1998). *Curr. Opin. Biotechnol.* **9**, 338–343.
Goldman, A., Ollis, D. L. & Steitz, T. A. (1987). *J. Mol. Biol.* **194**, 143–153.
Herbst-Irmer, R. & Sheldrick, G. M. (1998). *Acta Cryst.* B**54**, 443–449.
Hillig, R. C., Renault, L., Vetter, I. R., Drell, T. I., Wittinghofer, A. & Becker, J. (1999). *Mol. Cell*, **3**, 781–791.
Jeffrey, P. D., Strong, R. K., Sieker, L. C., Chang, C. Y., Campbell, R. L., Petsko, G. A., Haber, E., Margolies, M. N. & Sheriff, S. (1993). *Proc. Natl Acad. Sci. USA*, **90**, 10310–10314.
Jogl, G., Tao, X., Xu, Y. & Tong, L. (2001). *Acta Cryst.* D**57**, 1127–1134.
Jones, T. A., Cowan, S., Zou, J. Y. & Kjeldgaard, M. (1991). *Acta Cryst.* A**47**, 110–119.
Kahlenberg, V. V. (1999). *Acta Cryst.* B**55**, 745–751.
Larsen, N. A., Heine, A., de Prada, P., el Redwan, R., Yeates, T. O., Landry, D. W. & Wilson, I. A. (2002). *Acta Cryst.* D**58**, 2055–2059.
Laskowski, R. A., MacArthur, M. W., Moss, D. S. & Thornton, J. M. (1993). *J. Appl. Cryst.* **26**, 283–291.
Liang, A. G. W., Ealick, S., Nielsen, S., Schreiber, S. L. & Clardy, J. (1996). *Acta Cryst.* D**52**, 207–210.
Lietzke, S. E., Carperos, V. E. & Kundrot, C. E. (1996). *Acta Cryst.* D**52**, 687–692.
Luecke, H., Richter, H. T. & Lanyi, J. K. (1998). *Science*, **280**, 1934–1937.
Luzzati, V. (1952). *Acta Cryst.* **5**, 802–810.
Madden, D. R. (1995). *Annu. Rev. Immunol.* **13**, 587–622.
Matthews, B. W. (1968). *J. Mol. Biol.* **33**, 491–497.
Mazza, G., Housset, D., Piras, C., Gregoire, C., Lin, S. Y., Fontecilla-Camps, J. C. & Malissen, B. (1998). *Immunol. Rev.* **163**, 187–196.
Mueller, U., Muller, Y. A., Herbst-Irmer, R., Sprinzl, M. & Heinemann, U. (1999). *Acta Cryst.* D**55**, 1405–1413.
Mueller, U., Schubel, H., Sprinzl, M. & Heinemann, U. (1999). *RNA*, **5**, 670–677.
Otwinowski, Z. & Minor, W. (1997). *Methods Enzymol.* **276**, 307–326.
Rabijns, A., Verboven, C., Novoa de Armas, H., Van Damme, E. J., Peumans, W. J. & De Ranter, C. J. (2001). *Acta Cryst.* D**57**, 609–611.
Redinbo, M. R. & Yeates, T. O. (1993). *Acta Cryst.* D**49**, 375–380.
Rudolph, M. G., Kelker, M. S., Schneider, T. R., Yeates, T. O., Oseroff, V., Heidary, D. K., Jennings, P. A. & Wilson, I. A. (2003). *Acta Cryst.* D**59**, 290–298.
Rudolph, M. G. & Wilson, I. A. (2002). *Curr. Opin. Immunol.* **14**, 52–65.
Shawar, S. M., Vyas, J. M., Rodgers, J. R. & Rich, R. R. (1994). *Annu. Rev. Immunol.* **12**, 839–880.
Sheldrick, G. M. & Schneider, T. R. (1997). *Methods Enzymol.* **277**, 319–343.
Stroynowski, I. & Lindahl, K. F. (1994). *Curr. Opin. Immunol.* **6**, 38–44.
Taylor, H. O., O'Reilly, M., Leslie, A. G. & Rhodes, D. (2000). *J. Mol. Biol.* **303**, 693–707.
Terwisscha van Scheltinga, A. C., Valegard, K., Ramaswamy, S., Hajdu, J. & Andersson, I. (2001). *Acta Cryst.* D**57**, 1776–1785.
Tickle, I. J., Laskowski, R. A. & Moss, D. S. (1998). *Acta Cryst.* D**54**, 547–557.
Trame, C. B. & McKay, D. B. (2001). *Acta Cryst.* D**57**, 1079–1090.
Wingren, C., Crowley, M. P., Degano, M., Chien, Y. & Wilson, I. A. (2000). *Science*, **287**, 310–314.
Yang, F., Dauter, Z. & Wlodawer, A. (2000). *Acta Cryst.* D**56**, 959–964.
Yeates, T. O. (1988). *Acta Cryst.* A**44**, 142–144.
Yeates, T. O. (1997). *Methods Enzymol.* **276**, 344–358.
Yeates, T. O. & Fam, B. C. (1999). *Structure Fold. Des.* **7**, R25–R29.